Chapter 5

An improved volume power approach to estimate LAI from optimized dual-polarized SAR decomposition

5.1 Introduction

LAI is a critical parameter in studying terrestrial vegetation and its role in regulating global carbon, water, and energy cycles (Chen and Black, 1992; Fang et al., 2019; Singh et al., 2022). LAI measures the total surface area of leaves per unit of ground area. It is a dimensionless quantity. Remote sensing technology has played a vital role in producing long-term global LAI datasets that are widely used in various fields, including land–atmosphere interactions and the land surface carbon cycle (Knyazikhin et al., 1998). Precise measurement of LAI is essential for gaining insight into different ecological processes, such as the absorption of radiation, the maintenance of plant water balance, the interception of precipitation, and photosynthetic activity (Hill et al., 2006; Knyazikhin et al., 1998; Lafont et al., 2012; Zhu et al., 2013). Therefore, developing reliable and

efficient LAI estimation techniques using remote sensing data is significant in advancing our understanding of terrestrial vegetation and its impact on the global climate system.

PolSAR datasets are a very useful tool for earth observation as they allow for the characterization of different types of backscattered and the derivation of higher-level products. Over the years, many remarkable works have been published on polarimetric decomposition. Previous studies have proposed the decomposition of the target scattering matrix into three different orthogonal components (Cloude, 2009; Freeman and Durden, 1993; Lee and Pottier, 2009; Touzi et al., 2004; Zhang et al., 2017). In general, there are two kinds of decompositions: coherent and incoherent decompositions. The model-based incoherent decomposition approach developed by Freeman and Durden intends to extract information about the scattering processes using SAR images without requiring ground truth measurements (Freeman and Durden, 1993). The polarimetric coherency matrix is utilized for decomposing radar signals into three different scattering mechanisms, namely double-bounce, volume, and surface scatterings. Additionally, a fourth scattering mechanism proposed by Yamaguchi et al. from G4U (general four-component decomposition) has been introduced. These decompositions provide physical insight into the target surface (Yadav et al., 2022a; Yamaguchi et al., 2005, 2006). By decomposing radar signals into multiple independent components, polarimetric decomposition enables the relationship between these components and the properties of the scatterer. This technique can even sometimes provide better results than the optical results in differentiating the crops, despite having identical spectral signatures.

Apart from these, attempts have been made to utilize the eigen-based decomposition technique, namely Entropy-Anisotropy-Alpha ($H/\alpha/A$), for both dual-polarized and quad-polarized datasets (Cloude and Pottier, 1997; Guo et al., 2012; Zhang et al., 2013). However, most decomposition algorithms are made mainly for quad-pol data, which limits them from effectively being used in dual-polarization data. To address this limitation, Shan (Shan

et al., 2011) proposed a novel approach involving deriving unknown parameters, E, and ρ. The parameter E was derived from the invariant Hermitian matrix and has comparable characteristics with entropy (H). This study employs the outcomes of H-α decomposition to augment the results obtained through dual-polarized decomposition.

The degree of polarization (m) also plays a critical role in determining vegetation growth. Chang et al., 2018 developed a vegetation index (PRVI) using the m for quad-pol SAR data (Chang et al., 2018). They used the assumption that vegetation canopy acts as a depolarizing medium. This means that the polarization state of the electromagnetic waves that interact with the canopy becomes randomized, and the polarization information of the waves is lost. However, the depolarized portion of the signal is computed as $1 - m$, where m is the degree of polarization. Then, they multiplied it by the intensity of the cross-polarization channel (σ^0_{VH} in dB). This method resulted in a higher correlation of shrubland biomass with PRVI (R^2 = 0.75) than RVI (R^2 = 0.50). Shrub vegetation typically has random structures within the canopy. In contrast, crops often have a predefined orientation (e.g. vertical or horizontal based on electrophiles and planophiles), and crops are generally sown in rows. Depending solely on cross-polarized power can lead to backscatter intensity saturation issues. Therefore, including HV (or VH) may erroneously indicate a high vegetation index value, even if the vegetation canopy is not fully developed.

This study employed the Freeman-Durden decomposition technique to introduce a novel method for vegetation monitoring in dual-polarimetric SAR data. Building upon previous research in SAR-based vegetation analysis, this study proposes two key modifications to the Volume Power (VP) analysis technique. Firstly, m is incorporated into the analysis, leading to the development of Depolarized Volume Power (DVP). This enhancement is supported by literature on PolSAR studies, where researchers have highlighted the importance of the degree of polarization in vegetation scattering analysis (Dey et al., 2021; Yamaguchi et al., 2006). Secondly, the anisotropic scattering properties of vegetation are introduced,

which measures the directional distribution of the scattered energy and is particularly relevant for vertical vegetation, leading to the formulation of Anisotropic Volume Power (AVP). The significance of accounting for aniso-tropic scattering in SAR-based vegetation analysis has been demonstrated in the studies (Bai et al., 2021; Plank et al., 2017).

The modifications made in the VP analysis in this study, aim to reduce the impact of unwanted scattering mechanisms from the surface to the total scattering. This could be beneficial for various terrain types, as it addresses a common challenge in SAR data analysis. Moreover, these modifications collectively contributed to significant improvement in the accuracy of LAI estimation and also enhanced the sensitivity to vegetation scattering, thereby enabling more precise and efficient estimation of vegetation growth parameters.

5.2 Study area

The location in Figure 5.1 where this study is carried out belongs to the Gangetic plain of the Varanasi district of the Union of India. The reason behind the selection of this area is its location and climate. It is characterized by a wide range of temperatures that fluctuate from 7°C to 46°C throughout the year. Its extensive alluvial deposits make it one of the most fertile and agriculturally suitable land. The longitude and latitude of Varanasi are centered at$82^{\circ}58'56.92''$ E and $25^{\circ}15'55.27''$ N. This region observes an annual precipitation of about 1110 mm, in which the major contribution comes from the southwest monsoon, which typically dominates from July to September. Rice, wheat, sugarcane, and cotton are among the crops grown in the area, which benefit from the nutrient-rich soil and temperate temperature.

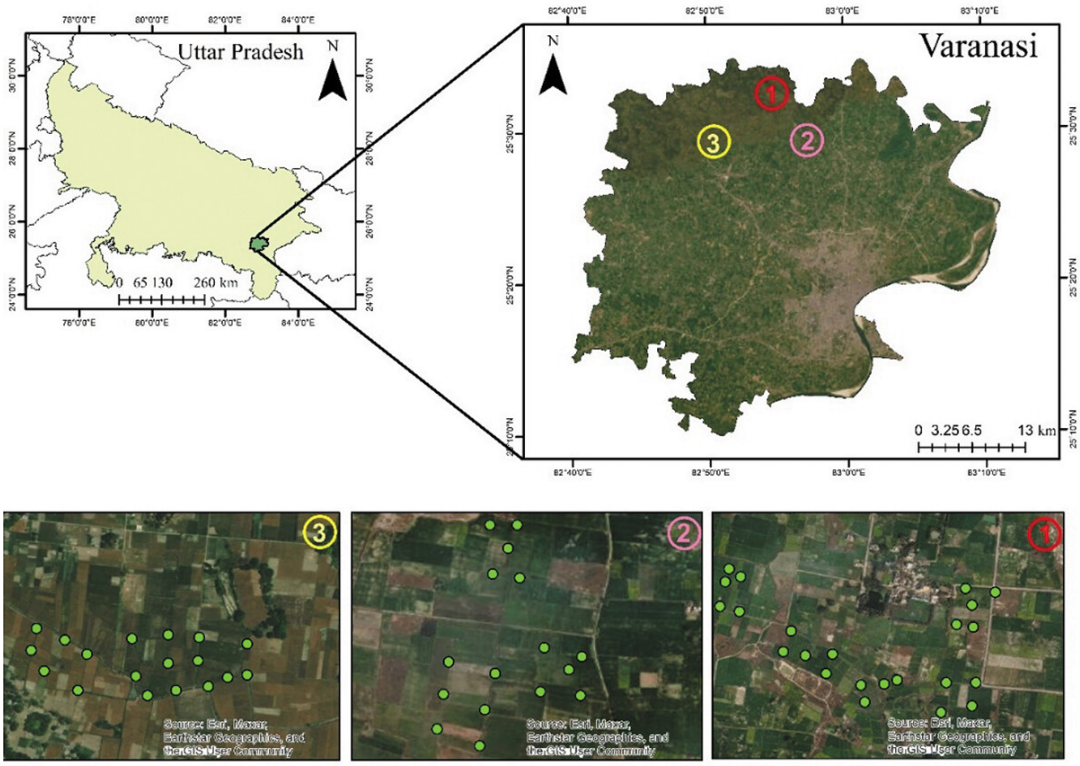

Figure 5.1 The image depicts three distinct study sites within the location.

5.3 Materials

5.3.1 Field sampling

Field measurements of LAI and plant height are conducted in a wheat field on three separate dates: January 10th, February 18th, and 7 March 2020, coincident with the flyovers of the Sentinel-1 satellite. On these three different dates, a total of 172 experimental points are established with a reasonably dispersed spatial distribution. Out of these points, 91 were employed for constructing the model, while 81 were reserved for validation purposes, as shown in Table 5.1. In this study, three distinct experimental sites are selected, and a detailed depiction of the distribution of the experimental points is shown in Figure 5.1. For each sampling site, a portable hand-held GPS receiver was utilized to determine the coordinates of longitude and latitude. To obtain the LAI data, the Li-COR plant canopy

analyzer (Li- Cor Inc.) is used in the study. Four measurements were taken below the plant canopy to get the final mean LAI data, and it was made sure that the device was functioning correctly. Additionally, the data collection process was conducted under sunny conditions to avoid potential contamination of the LAI data.

Table 5.1 Summary of in-situ measurements collected from three reference fields on three dates.

Location	**LAI (m2/m2) (min-max)**	**SM (m3/m3) (min-max)**	**Sampling point**	**Sampling date**
Region-1	0.56–5.81	0.08–0.97	62	10/01/2020,
Region-2	1.08–5.58	0.07–0.92	60	18/02/2020,
Region-3	0.98–6.21	0.08–0.96	50	07/03/2020

5.3.2 Satellite

The dual polarimetric C-band Sentinel-1 SLC dataset was used in Interferometric Wide (IW) mode to conduct crop monitoring. These datasets can be obtained free of charge from the Copernicus portal managed by the European Space Agency. The dataset is available in dual polarization, VV and VH. It has a temporal resolution of 12 days and a spatial resolution of 5 m × 20 m. The additional information regarding the Sentinel-1 datasets is shown in Table 5.2. The study utilized the SNAP 8.0 software, an open-source toolbox provided by ESA, to perform all necessary pre-processing steps of SLC data. These steps include calibration, speckle filtering, geometric correction, and matrix decomposition. Additionally, the QGIS toolbox, MATLAB, and Python 3.1 were used to carry out further analysis of the study.

Table 5.2 Characteristics of C- band Sentinel-1 SLC datasets used in the study.

Property of Sentinel-1 Image	Details
Data Acquisition Date	10-Jan-2020, 18-Feb-2020, 07-March-2020
Polarization	Dual (VV/VH)
Product Type	Level-1, SLC
Imaging frequency	C-band (5.4GHz)
Temporal resolution	06 days
Spatial Resolution	10m

5.4 Methods

5.4.1 Theoretical background

A scattering matrix is shown in Equation 5.1, is used to describe quad-pol information related to the polarization features of electromagnetic waves. The scattering matrix is also called the Sinclair matrix and can be expressed in terms of the H (horizontal) and V (vertical) linear polarization states.

$$\mathbf{S} = \begin{bmatrix} S_{\mathrm{HH}} & S_{\mathrm{HV}} \\ S_{\mathrm{VH}} & S_{\mathrm{VV}} \end{bmatrix} \tag{5.1}$$

A significant advancement in our comprehension of extracting physical surface information from the classical 2×2 coherent matrix $\mathbf{S}$ is the creation of system vectors. This method has proved helpful in various fields, such as linear algebra and signal processing. In this study, the vectorization of $\mathbf{S}$ is done as

$$\mathbf{k} = \frac{1}{2} trace\left([S]\Psi_p\right)$$

$$\mathbf{S} = \begin{bmatrix} S_{\mathrm{HH}} + S_{\mathrm{VV}} \\ S_{\mathrm{HH}} - S_{\mathrm{VV}} \\ S_{\mathrm{HV}} + S_{\mathrm{VH}} \\ i\,(S_{\mathrm{HH}} - S_{\mathrm{VV}}) \end{bmatrix} \tag{5.2}$$

Here S_{pq} (where p, q = H or V) is the scattering coefficient. Here p represents the transmitted polarization state, and q represents the received polarization of the electromagnetic energy in the HV polarimetric basis. The variable Ψ represents a set of 2×2 complex basis matrices, which are typically constructed to be orthonormal under some appropriate definition of the inner product. The operation Trace(...) involves adding up the diagonal elements of a matrix. Several variations of the basis combinations have been implemented in the literature, such as lexicographic and Pauli matrices. Here in this study, Pauli matrices (Equation 5.3) are used as a basis to generate a scattering vector

$$[\Psi_P] : \sqrt{2}\begin{bmatrix} 1 & 0 \\ 0 & 1 \end{bmatrix}, \sqrt{2}\begin{bmatrix} 1 & 0 \\ 0 & -1 \end{bmatrix}, \sqrt{2}\begin{bmatrix} 0 & 1 \\ 1 & 0 \end{bmatrix}, \sqrt{2}\begin{bmatrix} 0 & -i \\ i & 0 \end{bmatrix} \tag{5.3}$$

In the dual-polarimetric, (VV-VH) case, Equation 1 takes the form

$$\mathbf{S} = \begin{bmatrix} 0 & S_{\mathrm{HV}} \\ S_{\mathrm{VH}} & S_{\mathrm{VV}} \end{bmatrix} \tag{5.4}$$

The target vector k in the case of dual-polarized datasets (e.g. Sentinel-1) can be expressed as

$$\mathbf{S} = \frac{1}{\sqrt{2}} \begin{bmatrix} S_{\mathrm{VV}} + S_{\mathrm{HH}} & S_{\mathrm{VV}} - S_{\mathrm{HH}} \end{bmatrix}^T$$

or

$$\mathbf{S} = \frac{1}{\sqrt{2}} \begin{bmatrix} S_{\mathrm{VV}} & 2S_{\mathrm{VH}} \end{bmatrix}^T \tag{5.5}$$

Equation 5 represents the target vector for the dual-polarized case.

5.4.2 Freeman-Durden decomposition method

The Freeman-Durden decomposition method, consisting of three components, is created in 1998 by Freeman and Durden (Freeman and Durden, 1998). This method allows for the direct extraction of surface, dihedral, and volume scattering components from a coherent scattering matrix.

$$[T] = P_s[T]_{surface} + P_d[T]_{double} + P_v[T]_{volume} \tag{5.6}$$

where P_s, P_d and P_v are power of each scattering component.

$$[T_{surface}] = \begin{bmatrix} 1 & \beta & 0 \\ \beta^* & |\beta|^2 & 0 \\ 0 & 0 & 0 \end{bmatrix}, [T_{double}] = \begin{bmatrix} 1 & \alpha & 0 \\ \alpha^* & |\alpha|^2 & 0 \\ 0 & 0 & 0 \end{bmatrix}, [T_{double}] = \begin{bmatrix} 2 & 0 & 0 \\ 0 & 1 & 0 \\ 0 & 0 & 1 \end{bmatrix}$$

5.4.3 Odd-bounce and volume scattering

$$\mathbf{k_t} = \frac{1}{\sqrt{2}} \begin{bmatrix} S_{\mathrm{VV}} \\ 2S_{\mathrm{VH}} \end{bmatrix}$$

The outer product $k_t \times k_t$ gives

$$\mathbf{T} = \frac{1}{2}\begin{bmatrix} \langle |S_{VV}|^2 \rangle & \langle S_{VV} S_{VH}^* \rangle \\ \langle 2 S_{VH} S_{VV}^* \rangle & \langle 4 |S_{VH}|^2 \rangle \end{bmatrix} \tag{5.7}$$

$$\mathbf{T} = \begin{bmatrix} T_{11} & \langle T_{12} \\ T_{21} & \langle T_{22} \end{bmatrix} = P_s + P_v$$

$$[T] = P_s + P_v = f_s \begin{bmatrix} 1 & \beta^* \\ \beta & |\beta|^2 \end{bmatrix} + f_v \begin{bmatrix} 2 & 0 \\ 0 & 1 \end{bmatrix} \tag{5.8}$$

$$T_{11} = f_s + 2 f_v \tag{5.9}$$

$$T_{22} = |\beta|^2 f_s + 2 f_v \tag{5.10}$$

$$T_{12} = \beta^* f_s \tag{5.11}$$

Multiply with β in Equation 11

$$\beta T_{12} = |\beta|^2 f_s \tag{5.12}$$

From Equations 5.10 and 5.12

$$T_{22} = \beta T_{12} + f_v$$

$$f_v = T_{22} - \beta T_{12} \tag{5.13}$$

Now the equation system is simplified in two cases to ensure a uniquely solvable solution;

Case 1: when the surface scattering was dominant

$$\beta = \frac{T_{21}}{f_s} = \frac{T_{21}}{T_{11}}$$

From Equation 5.4

$$f_v = T_{22} - \frac{T_{21}}{T_{11}} T_{12}$$

$$f_v = T_{22} - \frac{|T_{12}|^2}{T_{11}} \tag{5.14}$$

Case: 2 dominant volume scattering,

$$f_v = T_{22} \tag{5.15}$$

$$f_s = T_{11} - 2T_{22} \tag{5.16}$$

The scattering power components Ps and PV of each scattering mechanism are derived as:

$$P = P_s + P_v = \left(|S_{HH}|^2 + 4|S_{VH}|^2\right) \tag{5.17}$$

$$|S_{VV}|^2 = |\beta|^2 f_s + f_v$$

$$|S_{VH}|^2 = f_v$$

Finally,

$$P_s = |\beta|^2 f_s \tag{5.18}$$

$$P_s = \frac{7}{3} f_v \tag{5.19}$$

In Equation 5.17, P is the total dual polarimetric power, which sums the surface power (P_s) and the volume power (P_v). The P_s is given by Equation 5.18, and P_v is given by Equation 5.19.

5.4.4 Decomposition for dual polarization

The scattering vector for this study is defined as Equation 1. The coherency matrix generated from the dual-polarized data is decomposed into the eigenvalues and eigenvectors matrix as

$$\langle T \rangle = \frac{1}{L} \sum_{i}^{L} k_i k_j^{dagger}$$

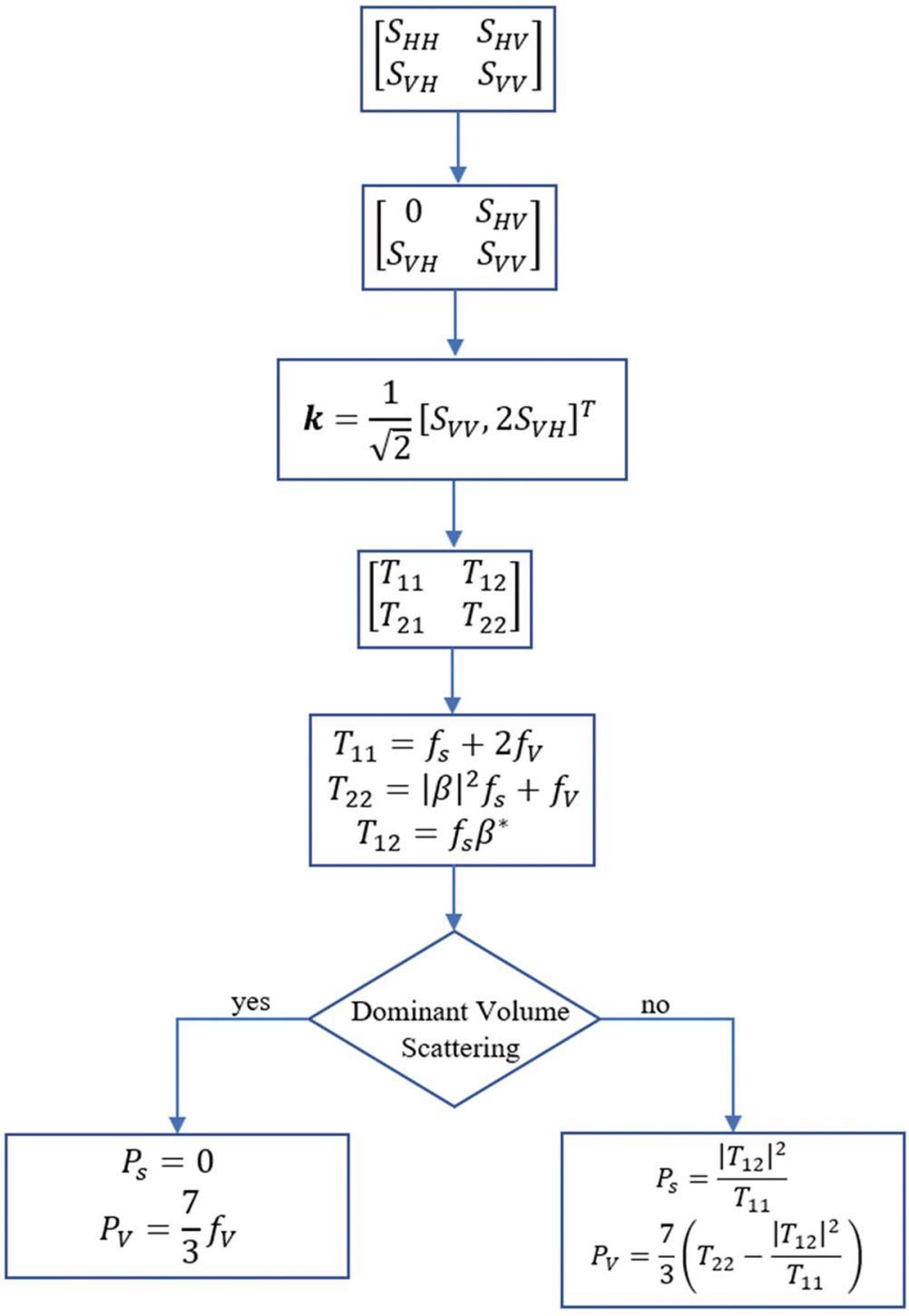

Figure 5.2 Calculation of scattering power components from modified Freeman-Durden decomposition.

Where L is the number of looks, which refers to the number of times a sensor or system 'looks' at a particular target or area, and † denotes the complex conjugate of a given value.

$$\langle T \rangle = \sum_{i=1}^{n} \lambda_i u_i u_i^T = U \begin{bmatrix} 1 & \beta & 0 \\ \beta^* & |\beta|^2 & 0 \\ 0 & 0 & 0 \end{bmatrix} U$$

$$u_i = [u_1 u_2]$$

Here n represents the polarimetric channels for dual polarimetric $n = 2$, $\lambda_1 \leq \lambda_2 \leq 0$ are eigenvalues, and U is an orthogonal unitary matrix with u_1 and u_2 as eigenvectors.

$$\overline{u_i} = e^{i\phi} \begin{bmatrix} cos\overline{\alpha} & sin\overline{\alpha} e^{i\delta_i} \end{bmatrix}; \alpha_i = cos^{-1}(|u_i|)$$

Where the variable ϕ is a physical quantity that is equivalent to the absolute phase of a target and α_i, δ_i are defined as.

$$\overline{\alpha} = \sum_{i=1}^{2} p_i \alpha_i; \overline{\delta} = \sum_{i=1}^{2} p_i \delta_i$$

When the coherency or covariance matrix is decomposed, it yields three parameters: entropy (H), scattering anisotropy (A), and mean scattering angle (α). These parameters are defined as follows:

$$H = -\sum_{i=1}^{n} p_i log_n P_i \tag{5.20}$$

$$P_i = \frac{\lambda_i}{\sum_{i=1}^{n} \lambda_i}$$

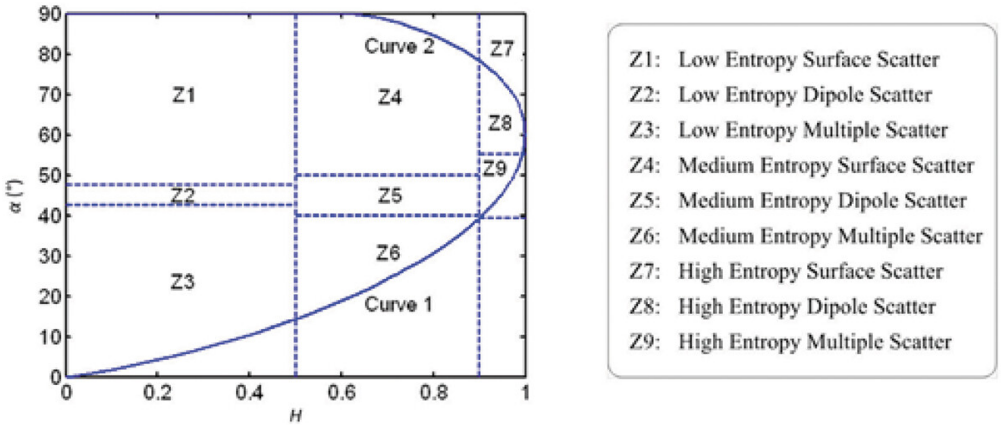

Figure 5.3 he $H-\alpha$ plane from full-polarization classification. It is divided into distinct zones corresponding to different physical properties.

Scattering anisotropy (also indicated as the degree of polarization) manifests the difference between the different scattering.

$$A = \frac{\lambda_1 - \lambda_2}{\lambda_1 + \lambda_2};\ 0 \leq A \leq 1 \tag{5.21}$$

The α parameter can distinguish between different types of scattering phenomenon, for example, surface scattering, double-bounce scattering, and volume scattering. The mean value was computed as

$$\overline{\alpha} = \sum_{i=1}^{2} p_i \alpha_i \tag{5.22}$$

$\overline{\alpha}$ values close to 0° Correspond to surface scattering, while values close to 45° and 90° Correspond to volume and dihedral scattering, respectively. By plotting $H-\alpha$ plane, it is possible to identify the scattering behavior of the target or structure being studied. Figure 5.3 illustrates the division of the $H-\alpha$ plane and the corresponding physical properties associated with each zone.

5.5 Definition of different volume power (VP) indices

The Freeman-Durden decomposition separates radar signals into two components: surface-related components and volume-related components. The surface-related contains information about the surface roughness, shape, and dielectric properties, while the volume-related component provides information about the vegetation canopy structure. Deriving the volume power from Freeman-Durden decomposition can provide valuable information about the vegetation canopy structure in a study area. In particular, the volume power component is proportional to the backscatter from the vegetation canopy and can be used to estimate the vegetation cover, height, and density. VP with additional information like degree of polarization and scattering anisotropy can provide improved accuracy and better characterization of the vegetation canopy structure, leading to more reliable results. The degree of polarization m measures the polarization state of the radar signal, which is related to the scattering properties of the target. It is the ratio of the difference between the maximum and minimum power of two orthogonal polarization states to their sum. Assuming that the radar signal is fully polarized, m can be used to modify the VP obtained from the Freeman-Durden decomposition. Specifically, the modified depolarized volume power (DVP) can be calculated as follows:

$$P_v^m(DVP) = (1-m)P_v \tag{5.23}$$

The rationale behind this modification is that $1-m$ represents the degree of depolarization, and it is directly related to the vegetation. By multiplying the VP by the $1-m$, we can account for the polarization-dependent scattering effects and obtain a more accurate estimate of the volume scattering component.

The other modification to the VP is achieved by scattering anisotropy. Scattering anisotropy is a measure of the directional dependence of the scattering mechanism, which

quantifies the degree to which the scattered radiation is concentrated in specific directions. This study is carried out over wheat, which has strong directional dependence. Assuming that the target is characterized by a single scattering mechanism, such as vegetation canopy, the modified AVP can be expressed as:

$$P_v^{m,A}(AVP) = \frac{1}{2}[(1-m)P_v + f(A)P_v] \tag{5.24}$$

and $f(A) = 1 + A + A^2 + A^3$ Where $f(A)$ is the scaling factor that depends on the scattering anisotropy A. This scaling factor accounts for the anisotropic nature of the canopy scattering, which is dominant by the double-bounce (A^2) and multiple-bounce (A^3) scattering between the leaves and branches. By multiplying the VP by the scaling factor, one can obtain a modified VP that accounts for the anisotropy of the scattering mechanism and provides a better estimate of the vegetation structure and biomass.

5.5.1 Volume power modeling

In this study, we model vegetation cover as a uniform dielectric slab to estimate the volume scattering. The suggested simplification is suitable for Sentinel-1 (which works at the C-band) since the depth at which the signal penetrates the medium and, therefore, the occurrence of multiple scattering is comparatively minor compared to that at the L-band. The model can be represented in the following manner:

$$P^0_{volumnepower} = \frac{Acos\theta}{2\kappa_e}(1-\tau^2_{vol}) \tag{5.25}$$

where $P^0_{volume;power}$ is total backscattering volume power, κ_e represents the coefficient of vegetation extinction and τ^2_{vol} is two-way transmissivity of the vegetation layer (Kirdiashev et al., 1979).

$$\tau_{vol}^2 = e^{-\frac{2\tau}{cos\theta}} \tag{5.26}$$

Nevertheless, several empirical relations between the τ and crop biophysical parameters (LAI and VWC) have been established (Jackson and O'Neill, 1990). So

$$\tau = B * LAI \tag{5.27}$$

B represents an empirical variable (Jackson and Schmugge, 1991; Kirdiashev et al., 1979; Ulaby and Wilson, 1985). The relationship between the variable τ, crop height (h), and extinction coefficient κ_e is determined by the properties of the medium through which electromagnetic radiation travels. The variables are related as follows:

$$\tau = \kappa_e * h \tag{5.28}$$

Using Equations 5.15 - 5.18, the volume power can be rewritten as

$$P^0_{volumnepower} = \frac{Acos\theta}{2BLAI} h \left(1 - e^{-\frac{2BLAI}{cos\theta}}\right) \tag{5.29}$$

The parameters A and B in the model are empirical constants. For an accurate calculation of the parameter A, which indicates the volume scattering, it is necessary to have a thorough understanding of the plant canopy. To calculate the parameters A and B for a specific crop, it is essential to fit Equation 5.29 to measurements collected from field data. After this is accomplished, it is presumed that A and B remain constant for that crop type throughout the same development stage. The next subsection describes the model parametrization, estimation of A and B parameters, and inversion.

5.5.2 Model parametrization and inversion

In the present study, the parametrization of the model (Equation 5.29) for accurate simulation of VP is done. This is achieved by estimating the unknown parameters A and b using in-situ data, including LAI and crop height. The total pooled datasets are divided into a training set (70%) and a testing set (30%) for model parameterization and validation purposes, respectively. To validate the model, an independent dataset of crops is employed. A non-linear least square minimization process is applied to the cost function Equation 5.30, which is designed to minimize the discrepancy between simulated and actual values of VP. The obtained values of A and b enabled the accurate simulation of VP.

$$cost\,function = \sum_{i} (VP_{calculated} - VP_{simulated})_i \tag{5.30}$$

Table 5.3 Estimated values of model parameters a and b for different volume powers.

Parameters	FDVP	DVP	AVP
A	0.0061	0.0048	0.0039
B	0.3510	0.3745	0.3115

The parameters A and B, along with VP as defined by the relevant equations, are utilized to invert Equation 5.29 for LAI retrieval. The model parameters obtained from the non-linear least square minimization process are shown in Table 5.3

5.6 Results

5.6.1 H-alpha decomposition for dual polarization

Figure 5.4 shows the alpha vs. entropy plot from the eigen-based decomposition. This decomposition is divided into different zones based on the physical scattering phenomenon, and the zones are explained in figure 5.3. As the Sentinel-1 dual polarimetric data lacks VV

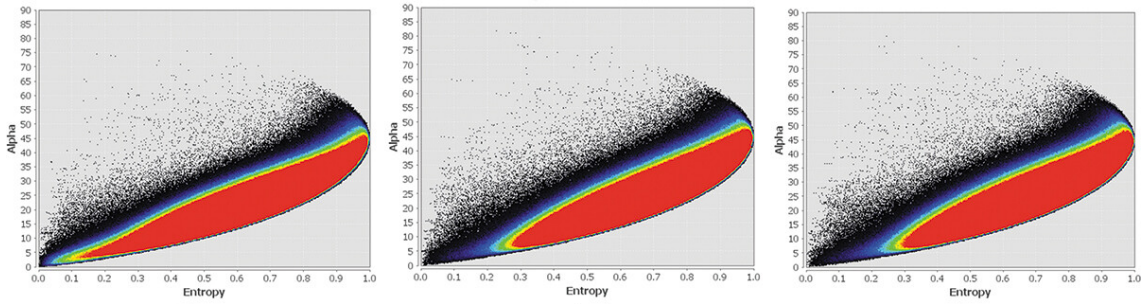

Figure 5.4 Temporal variation of the decomposition parameters entropy and alpha of the study region.

polarization, the upper zones of the plot do not contain relevant information. Consequently, figure 5.4 primarily comprises data from zone 1 (Z1), zone 2 (Z2), zone 4 (Z4), zone 5 (Z5), and zone 8 (Z8). Red indicates a higher pixel density, while black indicates a lower pixel density. Figure 5.4 shows that the pixel density in Z3 decreases over time, implying a decrease in low-entropy multiple scattering, which in turn suggests a decrease in surface (bare) scattering. It is also shown that for an alpha value of 30°-45°, which typically corresponds to the volume scattering, in the Z5, Z6, and Z9, the pixel density indicates that the region has a high vegetation percentage due to which in this region medium entropy multiple and dipole scattering is prominent.

5.6.2 Calculation of degree of polarization

The use of Sentinel-1 data in this study calculates the m of pixels located within the three sites of the study region. In accordance with the methodology put forth by Chang et al. (2018) in their derivation of the PRVI vegetation index, vegetation canopies are regarded as depolarizing media, thereby resulting in a depolarized component that is obtained by subtracting the m from unity (i.e. $(1-m)$). Our analysis demonstrates that the m values, as represented by the pixel values of the sites in the study region, exhibit a decrement over time, signifying the growth of vegetation in the area, as shown in Figure 5.5(b). Additionally, a box and whiskers plot (Figure 5.5(a)) was created to illustrate the

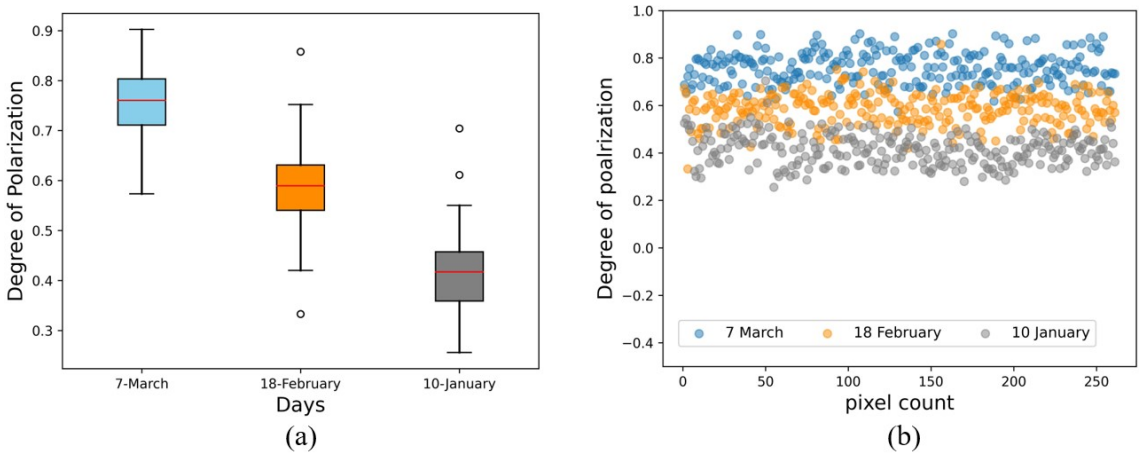

Figure 5.5 Degree of polarization over three study dates for the study pixels over study region.

distribution of m values across different dates. The box and whisker plot is a helpful tool that provides valuable information about the variability of the data, including the median, quartiles, and outliers. In Figure 5.5(a), it is shown that the median and the range of the m decreased over time. This finding aligns with the established principle that the reduction in m can serve as a proxy for vegetation growth. The PRVI vegetation index developed leverages this concept by quantifying the extent of vegetation in a specific area. The assumption that vegetation canopies depolarize radar signals enables the calculation of the depolarized portion of the signal, thus providing a means of monitoring vegetation growth and changes over time. Notably, a decrease in the m has been observed in the study region, indicative of thriving vegetation in the area. This observation has practical implications in a multitude of fields, including agriculture, forestry, and land use management. It serves as a valuable tool in monitoring shifts in vegetation cover in the region.

5.6.3 Volume power characterization

The volume power of vegetation in the study area is a critical aspect of understanding its structure and growth. This section presents an in-depth analysis of volume power characterization using m and anisotropy. The evolution of vegetation growth in the study

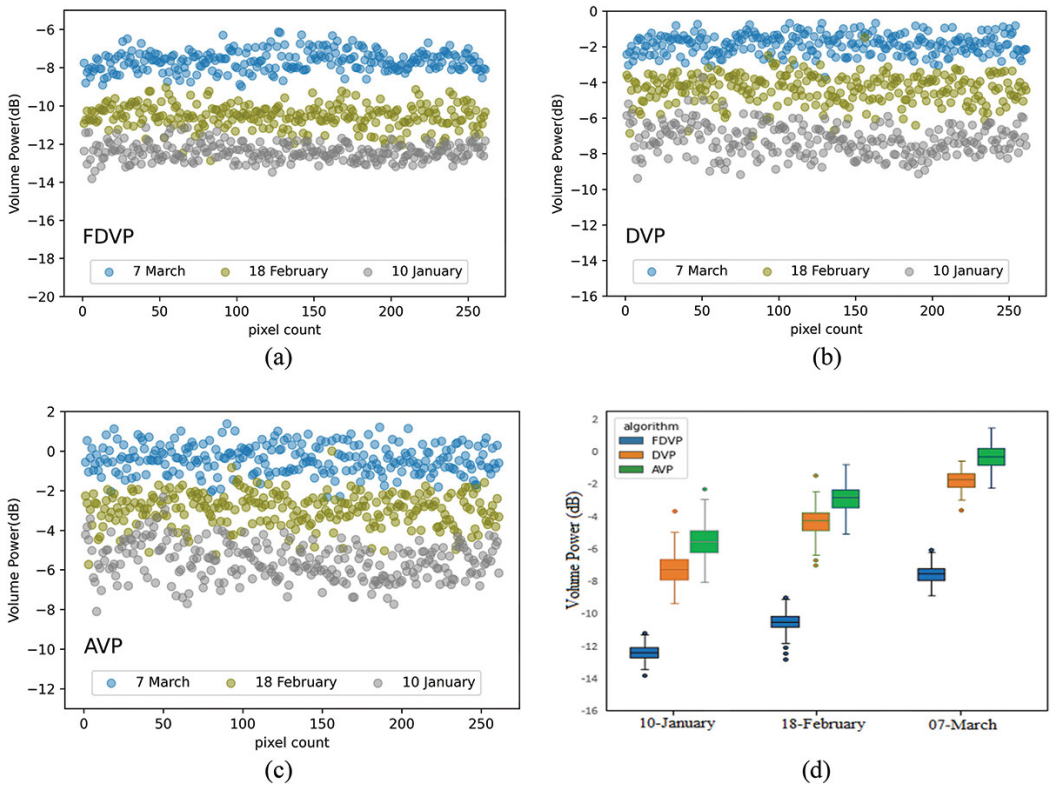

Figure 5.6 This figure displays the variations in the volume power behavior of pixels within the designated study region for three different algorithms: (a) FDVP, (b) DVP, and (c) AVP.

region is effectively captured in Figure 5.6, which displays the behavior of VP, DVP, and AVP across three dates. Figure 5.6 shows an apparent increase in the values of VP, DVP, and AVP as the vegetation grows, providing valuable insights into the dynamics of vegetation development in the region. By combining the m and scattering anisotropy with the VP, we calculated the values of DVP and AVP, resulting in a more distinct representation of vegetation growth over time. Figure 5.6(c), which illustrates the AVP change across three dates of the study region, shows more pronounced and provides a clearer picture of the vegetation development in the study region. AVP is more sensitive to vegetation cover, and variation in vegetation features is also prominent. Additionally, Figure 5.6(d) is created to compare the performance of all three algorithms collectively and effectively using the box and whiskers plot. The box plot in Figure 5.6(d) is organized such that the VP calculated using each algorithm for each study date is grouped together. This allows

for a comparison of the sensitivity of the different algorithms over time. The results of this analysis indicate that the VP calculated using the FDVP algorithm is less sensitive than the other two algorithms (i.e. the AVP and the FDVP) for all three dates. This means that changes in vegetation growth may not be as accurately captured by the FDVP algorithm compared to the other two. On the other hand, the VP calculated using the AVP algorithm has shown better sensitivity than the other two algorithms. This suggests that the AVP algorithm may be better suited for detecting changes in vegetation growth over time in the study region.

5.6.4 Analysis of VP, DVP, and AVP and retrieval of LAI

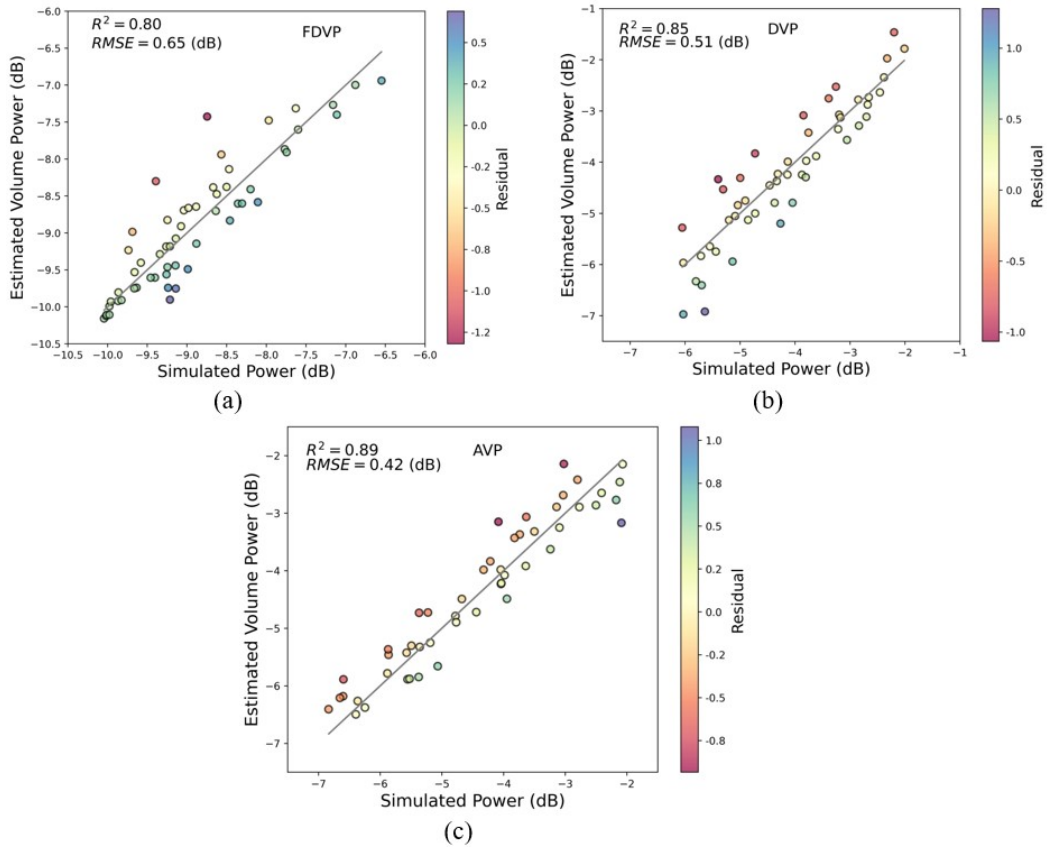

Figure 5.7 Illustrates a comparison between the estimated and simulated volume power within the study region, as obtained through the use of three different imaging techniques: (a) FDVP, (b) DVP and (c) AVP.

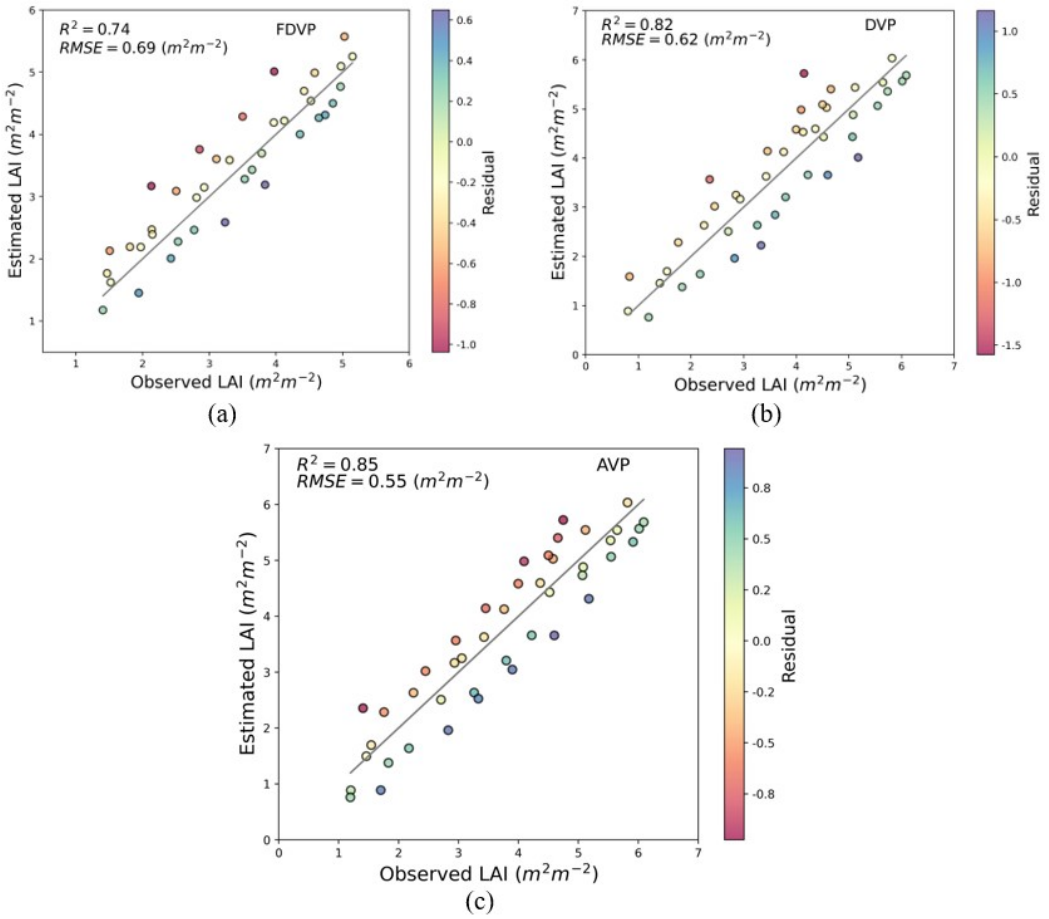

Figure 5.8 The leaf area index (LAI) results were obtained through the use of three different techniques: (a) FDVP, (b) DVP and (c) AVP.

The present study is focused on the improvement of the VP through the modifications for the retrieval of the vegetation parameters. To validate the accuracy of the model, a thorough evaluation process is conducted using an independent dataset of LAI and plant height obtained from field measurements which is not utilized in the model's parameterization process.

The VP calculated through FDVP, DVP, and AVP are plotted against the VP simulated from the model (Equation 5.29). The results are shown in Figure 5.7. These figures indicate a significant improvement in DVP and AVP as compared to FDVP. The values of R^2 and RMSE were found better for AVP (0.89, 0.42 (dB)), and DVP (0.85, 0.51 (dB)) than FDVP (0.80, 0.65(dB)). In Figure 5.8, the sampled LAI recorded at a time close to Senitnel-1

overpasses, and LAI retrieved using the VP, DVP, and AVP algorithms are compared. As presented in Figure 5.8, the performance of different scaled volume power metrics and models are evaluated. The comparison of the LAI values obtained from these metrics with the independent dataset of LAI provided valuable insights into the effectiveness of each metric. The LAI values retrieved from AVP are more accurate than the other two because they represent the average condition of the entire field. The R^2 and RMSE error between the sampled and retrieved LAI from FDVP, DVP, and AVP are respectively (0.74, 0.69(m^2m^{-2})), (0.82, 0.62(m^2m^{-2})), (0.85; 0.55(m^2m^{-2})).

5.7 Conclusion

This study provided a new method for estimating vegetation properties, specifically LAI, using dual polarimetric SAR data. This method combined the volume power component of the Freeman-Durden decomposition with the degree of polarization to derive the Depolarized-Volume Power and Anisotropic-Volume Power metrics, which are then used to estimate LAI. The proposed approach has demonstrated that the addition of anisotropy information resulted in better estimation, particularly for crops that are grown in a systematic manner, such as wheat. The advantage of using the volume power metric from the decomposition technique over traditional scattering models is that it provides more detailed information about the vegetation structure and properties. Traditional scattering models rely on assumptions about the shape and size of vegetation elements, which sometimes can lead to inaccuracies in the estimates of vegetation properties. In contrast, the volume power metric from decomposition techniques like the Freeman- Durden decomposition provides a direct measure of the volume scattering (vegetation), which is less dependent on assumptions about the shape and size of vegetation elements. This can lead to more accurate estimates of vegetation properties, such as biomass and leaf area index, which are essential for various applications in agriculture, forestry, and environmental monitoring.

While this work mainly focused on the volume decomposition part of the Freeman-Durden decomposition, further enhancement in the surface properties can also be achieved by using the surface and double scattering components. For example, the surface scattering component of the decomposition can provide information about the type and condition of the underlying surface, such as soil moisture and roughness. Overall, the approach presented in this study has the potential to significantly improve our understanding of vegetation properties and dynamics and has a wide range of applications in fields such as ecology, forestry, and agriculture.